LEARNING TO INDUCE CAUSAL STRUCTURE

Anonymous authors
Paper under double-blind review

ABSTRACT

The fundamental challenge in causal induction is to infer the underlying graph structure given observational and/or interventional data. Most existing causal induction algorithms operate by generating candidate graphs and evaluating them using either score-based methods (including continuous optimization) or independence tests. In our work, we instead treat the inference process as a black box and design a neural network architecture that learns the mapping from *both observational and interventional data* to graph structures via supervised training on synthetic graphs. The learned model generalizes to new synthetic graphs, is robust to train-test distribution shifts, and achieves state-of-the-art performance on naturalistic graphs for low sample complexity.

1 INTRODUCTION

The problem of discovering the causal relationships that govern a system through observing its behavior, either passively (*observational data*) or by manipulating some of its variables (*interventional data*), lies at the core of many scientific disciplines, including medicine, biology, and economics. By using the graphical formalism of causal Bayesian networks (CBNs) (Koller & Friedman, 2009; Pearl, 2009), this problem can be framed as inducing the graph structure that best represents the relationships. Most approaches to causal structure induction are based on an unsupervised learning paradigm in which the structure is directly inferred from the system observations, either by ranking different structures according to some metrics (score-based approaches) or by determining the presence of an edge between pairs of variables using conditional independence tests (constraint-based approaches) (Drton & Maathuis, 2017; Glymour et al., 2019; Heinze-Deml et al., 2018a;b) (see Fig. 1(a)). The unsupervised paradigm poses however some challenges: score-based approaches are burdened with the high computational cost of having to explicitly consider all possible structures and with the difficulty of devising metrics that can balance goodness of fit with constraints for differentiating causal from purely statistical relationships (e.g. sparsity of the structure or simplicity of the generation mechanism); constraint-based methods are sensitive to failure of independence tests and require faithfulness, a property that does not hold in many real-world scenarios (Koski & Noble, 2012; Mabrouk et al., 2014).

Recently, supervised learning methods based on observational data have been introduced as an alternative to unsupervised approaches (Lopez-Paz et al., 2015a;b; Li et al., 2020). In this work, we extend the supervised learning paradigm to also use interventional data, enabling greater flexibility. We propose a model that is first trained on synthetic data generated using different CBNs to learn a mapping from data to graph structures and then used to induce the structures underlying datasets of interest (see Fig. 1(b)). The model is a novel variant of a transformer neural network that receives as input a dataset consisting of observational and interventional samples corresponding to the same CBN and outputs a prediction of the CBN graph structure. The mapping from the dataset to the underlying structure is achieved through an attention mechanism which alternates between attending to different variables in the graph and to different samples from a variable. The output is produced by a decoder mechanism that operates as an autoregressive generative model on the inferred structure. Our approach can be viewed as a form of meta-learning, as the model learns about the relationship between datasets and structures underlying them.

A requirement of a supervised approach would seem to be that the distributions of the training and test data match or highly overlap. Obtaining real-world training data with a known causal structure that matches test data from multiple domains is extremely challenging. We show that meta-learning enables the model to generalize well to data from naturalistic CBNs even if trained on synthetic

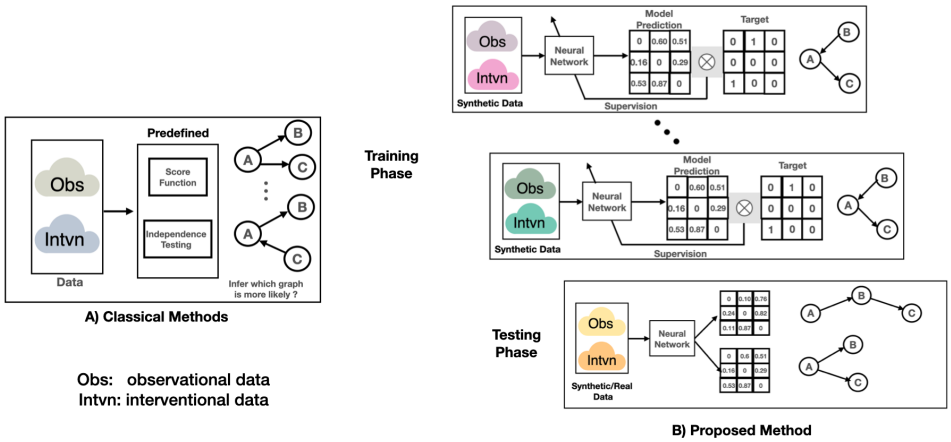

Figure 1: (A). Standard unsupervised approach to causal structure induction: Algorithms use a predefined scoring metric or statistical independence tests to select the best candidate structures. (B). Our supervised approach to causal structure induction (via attention; CSIvA): A model is presented with data and structures as training pairs and learns a mapping between them.

data with relatively few assumptions. We show that our model can learn a mapping from datasets to structures and achieves state-of-the-art performance on classic benchmarks such as the Sachs, Asia and Child datasets (Lauritzen & Spiegelhalter, 1988; Sachs et al., 2005; Spiegelhalter & Cowell, 1992), despite never directly being trained on such data. Our contributions can be summarized as follows:

- We tackle causal structure induction with a supervised approach (CSIvA) that maps datasets composed of *both observational and interventional* samples to structures.
- We introduce a variant of a transformer architecture whose attention mechanism is structured to discover relationships among variables across samples.
- We show that CSIvA generalizes to novel structures, whether or not training and test distributions match. Most importantly, training on synthetic data transfers effectively to naturalistic CBNs.
- We show that CSIvA significantly outperforms state-of-the-art causal discovery methods such as DCDI (Brouillard et al., 2020), ENCO (Lippe et al., 2021) both on various types of synthetic CBNs, as well as on naturalistic CBNs.

2 Background

In this section we give some background on causal Bayesian networks and transformer neural networks, which form the main ingredients of our approach (see Appendix A.1 for more details).

Causal Bayesian networks (CBNs). A *causal Bayesian network* (Koller & Friedman, 2009; Pearl, 2009) is a pair $\mathcal{M} = \langle \mathcal{G}, p \rangle$, where $\mathcal{G}$ is a *directed acyclic graph* (DAG) whose nodes $X_1, \ldots, X_N$ represent random variables and edges express casual dependencies among them, and where p is a joint distribution over all nodes such that $p(X_1, \ldots, X_N) = \prod_{n=1}^{N} p(X_n \mid \mathrm{pa}(X_n))$, where $\mathrm{pa}(X_n)$ are the *parents* of X_n, i.e. the nodes with an edge onto X_n (direct causes of X_n). An input to the transformer neural network is formed by a dataset $\mathcal{D} = \{x^s\}_{s=1}^{S}$, where $x^s := (x_1^s, \ldots, x_N^s)^\mathsf{T}$ is either an *observational data sample* or an *interventional data sample* obtained by performing an intervention on a randomly selected node in $\mathcal{G}$. Observational data samples are samples from $p(X_1, \ldots, X_N)$. Except where otherwise noted, for all experimental settings, we considered *hard interventions* on a node X_n that consist in replacing the conditional probability distribution (CPD) $p(X_n \mid \mathrm{pa}(X_n))$ with a delta function $\delta_{X_{n'}=x}$ forcing $X_{n'}$ to take on value x. Additional experiments were also performed using *soft interventions*, which consisted of replacing $p(X_n \mid \mathrm{pa}(X_n))$ with a different CPD $p'(X_n \mid \mathrm{pa}(X_n))$. An *interventional data sample* is a sample from $\delta_{X_{n'}=x} \prod_{n=1, n\neq n'}^{N} p(X_n \mid \mathrm{pa}(X_n))$ in the first case, and a sample from $p'(X_n \mid \mathrm{pa}(X_n)) \prod_{n=1, n\neq n'}^{N} p(X_n \mid \mathrm{pa}(X_n))$ in the second case. The structure of $\mathcal{G}$ can be represented by an adjacency matrix A, defined by setting the (k, l) entry, $A_{k,l}$, to 1 if there is an edge from

X_l to X_k and to 0 otherwise. Therefore, the n-th row of A, denoted by $A_{n,:}$, indicates the parents of X_n while the n-th column, denoted by $A_{:,n}$, indicates the *children* of X_n.

Transformer neural network. A transformer (Devlin et al., 2018; Vaswani et al., 2017) is a neural network equipped with layers of self-attention that make them suited to modelling structured data. In traditional applications, attention is used to account for the sequentially ordered nature of the data, e.g. modeling a sentence as a stream of words. In our case, each input of the transformer is a dataset of observational or interventional samples corresponding to the same CBN. Attention is thus used to account for the structure induced by the CBN graph structure and by having different samples from the same node. Transformers are permutation invariant with respect to the positions of the input elements, ensuring that the graph structure prediction does not depend on node and sample position.

3 Causal Structure Induction via Attention (CSIvA)

Our approach is to treat causal structure induction as a supervised learning problem, by training a neural network to learn to map *observational and interventional* data to the graph structure of the underlying CBN. Obtaining diverse, real-world data with known causal relationships in amounts sufficient for supervised training is not feasible. The key contribution of this work is to introduce a method that uses synthetic data generated from CBNs with different graph structures and associated CPDs that is robust to shifts between the training and test data distributions.

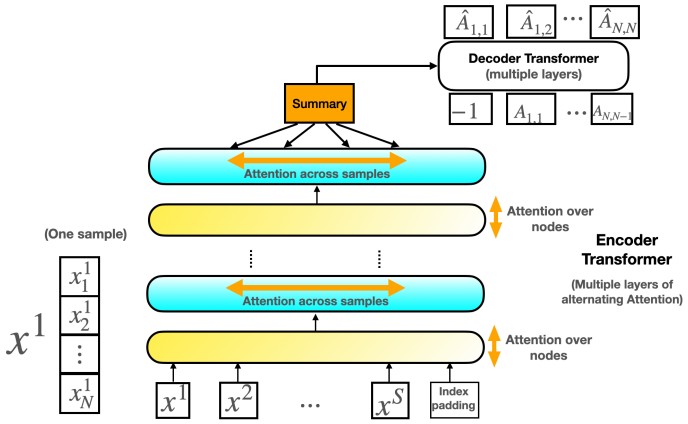

Figure 2: Our model architecture and the structure of the input and output at training time. The input is a dataset $\mathcal{D} = \{x^s := (x_1^s, \dots, x_N^s)^\mathsf{T}\}_{s=1}^S$ of S samples from a CBN and its adjacency matrix A. The output is a prediction $\hat{A}$ of A.

3.1 Supervised approach

We learn a distribution of graphs conditioned on observational and interventional data as follows. We generate training data from a joint distribution $t(\mathcal{G}, \mathcal{D})$, between a graph $\mathcal{G}$ and a dataset $\mathcal{D}$ comprising of S *observational* and *interventional* samples from a CBN associated to $\mathcal{G}$ as follows. We first sample a set of graphs $\{\mathcal{G}^i\}_{i=1}^I$ with nodes $X_1^i, \dots, X_N^i$ from a common distribution $t(\mathcal{G})$ as described in Section 4 (to simplify notation, in the remainder of the paper we omit the graph index i when referring to nodes), and then associate random CPDs to the graphs as described in Section 4. This results in a set of CBNs $\{\mathcal{M}^i\}_{i=1}^I$. For each CBN $\mathcal{M}^i$, we then create a dataset $\mathcal{D}^i = \{x^s\}_{s=1}^S$, where each element $x^s := (x_1^s, \dots, x_N^s)^\mathsf{T}$ is either an observational data sample or an *interventional* data sample obtained by performing an intervention on a randomly selected node in $\mathcal{G}^i$.

Our model defines a distribution $\hat{t}(\mathcal{G} \,|\, \mathcal{D}; \Theta)$ over graphs conditioned on observational and *interventional* data and parametrized by Θ. Specifically, $\hat{t}(A \,|\, \mathcal{D}; \Theta)$ has the following auto-regressive form: $\hat{t}(A \,|\, \mathcal{D}; \Theta) = \prod_{l=1}^{N^2} \sigma(A_l; \hat{A}_l = f_\Theta(A_{1,\dots,(l-1)}, \mathcal{D}))$, where $\sigma(\cdot; \rho)$ is the Bernoulli distribution with parameter ρ, which is a function f_Θ built from an encoder-decoder architecture explained in Section 3.2 taking as input previous elements of the adjacency matrix A (represented here as an array of N^2 elements) and $\mathcal{D}$. It is trained via maximum likelihood estimation (MLE), i.e $\Theta^* = \text{argmin}_\Theta \mathcal{L}(\Theta)$, where $\mathcal{L}(\Theta) = -\mathbb{E}_{(\mathcal{G},\mathcal{D})\sim t}[\ln \hat{t}(\mathcal{G} \,|\, \mathcal{D}; \Theta)]$, which corresponds to the usual cross-entropy (CE) loss for the Bernoulli distribution. Training is achieved using a stochastic gradient descent (SGD) approach in which each gradient update is performed using a pair $(\mathcal{D}^i, A^i)$. The data-sampling distribution $t(\mathcal{G}, \mathcal{D})$ and the MLE objective uniquely determine the target distribution learned by the model. In the infinite capacity case, $\hat{t}(\cdot \,|\, \mathcal{D}; \Theta^*) = t(\cdot \,|\, \mathcal{D})$. To see this, it suffices to note that the MLE objective $\mathcal{L}(\Theta)$ can be written as $\mathcal{L}(\Theta) = \mathbb{E}_{\mathcal{D}\sim t}[\text{KL}(\hat{t}(\cdot \,|\, \mathcal{D}; \Theta); t(\cdot \,|\, \mathcal{D}))] + c$, where KL is the Kullback-Leibler divergence and c is a constant. In the finite-capacity case, the distribution defined by the model $\hat{t}(\cdot \,|\, \mathcal{D}; \Theta^*)$ is only an approximation of $t(\cdot \,|\, \mathcal{D})$.

3.2 MODEL ARCHITECTURE

The function f_Θ defining the model's probabilities is built using two transformer networks. It is formed by an encoder transformer and by a decoder transformer (which we refer to as "encoder" and "decoder" for short). At training time, the encoder receives as input dataset $\mathcal{D}^i$ and outputs a representation that summarizes the relationship between nodes in $\mathcal{G}^i$. The decoder then recursively outputs predictions of the elements of the adjacency matrix A^i using as input the elements previously predicted and the encoder output. This is shown in Fig. 2 (where we omitted index i, as in the remainder of the section). At test time we obtain deterministic predictions of the adjacency matrix elements by taking the argmax of the Bernoulli distribution for use as inputs to the decoder.

3.2.1 ENCODER

Our encoder is structured as an $(N+1) \times (S+1)$ lattice. The $N \times S$ part of the lattice formed by the first N rows and first S columns receives a dataset $\mathcal{D} = \{(x_1^s, \ldots, x_N^s)^\mathsf{T}\}_{s=1}^S$. This is unlike standard transformers which typically receive as input a single data sample (e.g., a sequence of words in neural machine translation applications) rather than a set of data samples. Row $N+1$ of the lattice is used to specify whether each data sample is *observational*, through value -1, or *interventional*, through integer value in $\{1, \ldots, N\}$ to indicate the intervened node.

The goal of the encoder is to infer causal relationships between nodes by examining the set of samples. The transformer performs this inference in multiple stages, each represented by one transformer layer, such that each layer yields a $(N+1) \times (S+1)$ lattice of representations. The transformer is designed to deposit its summary representation of the causal structure in column $S+1$.

Embedding of the input. Each data-sample element x_n^s is embedded into a vector of dimensionality H. Half of this vector is allocated to embed the value x_n^s itself, while the other half is allocated to embed the unique identity for the node X_n. The value embedding is obtained by passing x_n^s, whether discrete or continuous, through an MLP[1] encoder specific to node X_n. We use a node-specific embedding because the values of each node may have very different interpretations and meanings. The node identity embedding is obtained using a standard 1D transformer positional embedding over node indices. For column $S+1$ of the input, the value embedding is a vector of zeros.

Alternating attention. Traditional transformers discover relationships among the elements of a data sample arranged in a one-dimensional sequence. With our two-dimensional lattice, the transformer could operate over the entire lattice at once to discover relationships among both nodes and samples. Given an encoding that indicates position n, s in the lattice, the model can in principle discover stable relationships among nodes over samples. However, the inductive bias to encourage the model to leverage the lattice structure is weak. Additionally, the model is invariant to sample ordering, which is desirable because the samples are *iid*. Therefore, we arrange our transformer in alternating layers. In the first layer of the pair, attention operates across all nodes of a single sample $(x_1^s, \ldots, x_N^s)^\mathsf{T}$ to encode the relationships among two or more nodes. In the second layer of the pair, attention operates across all samples for a given node $(x_n^1, \ldots, x_n^S)$ to encode information about the distribution of node values. Alternating attention in transformers was also done in Kossen et al. (2021).

Encoder summary. The encoder produces a *summary* vector e_n^{sum} with H elements for each node X_n, which captures essential information about the node's behavior and its interactions with other nodes. The summary representation is formed independently for each node and involves combining information across the S samples (the columns of the lattice). This is achieved with a method often used with transformers that involves a weighted average based on how informative each sample is. The weighting is obtained using the embeddings in column $S+1$ to form queries, and embeddings in columns $1, \ldots, S$ to provide keys and values, and then using standard key-value attention.

3.2.2 DECODER

The decoder uses the summary information from the encoder to generate a prediction of the adjacency matrix A of the underlying $\mathcal{G}$. It operates sequentially, at each step producing a binary output indicating the prediction $\hat{A}_{k,l}$ of $A_{k,l}$, proceeding row by row. The decoder is an autoregressive

[1] Using an MLP for a discrete variable is a slightly inefficient implementation of a node value embedding, but it ensures that the architecture is general.

transformer, meaning that each prediction $\hat{A}_{kl}$ is obtained based on all elements of A previously predicted, as well as the summary produced by the encoder. Our method does not enforce acyclicity. Although this could in principle yield cycles in the graph, in practice we observe strong performance regardless (Section 6.4), likely due to the fact that training and evaluation graphs typically studied (e.g., ER-1 and ER-2) are very sparse. Nevertheless, one could likely improve the results e.g. by using post-processing (Lippe et al., 2021) or by extending the method with an accept-reject algorithm (Castelletti & Mascaro, 2022; Li et al., 2022).

Auxiliary loss. We found that autoregressive decoding of the flattened $N \times N$ adjacency matrix is too difficult for the decoder to learn alone. To provide additional inductive bias to facilitate learning of causal graphs, we added the auxiliary task of predicting the parents $A_{n,:}$ and children $A_{:,n}$ of node X_n from the encoder summary, e_n^{sum}. This is achieved using an MLP to learn a mapping f_n, such that $f_n(e_n^{\text{sum}}) = (\hat{A}_{n,:}, \hat{A}_{:,n}^{\mathsf{T}})$. While this prediction is redundant with the operation of the decoder, it short-circuits the autoregressive decoder and provides a strong training signal to support proper training.

4 SYNTHETIC DATA

In this section, we discuss identifiability and describe how synthetic data were generated for training and testing in Sections 6.1 and 6.2, and training in Section 6.3.

Identifiability. Dataset $\mathcal{D}^i$ associated to CBN $\mathcal{M}^i$ is given by $\mathcal{D}^i = \{x^s\}_{s=1}^S$, where $x^s := (x_1^s, \dots, x_N^s)^{\mathsf{T}}$ is either an observational or interventional data sample obtained by performing a hard intervention on a randomly selected node in $\mathcal{G}^i$. As discussed in Eberhardt et al. (2006), in the limit of an infinite amount of such single-node interventional data samples, $\mathcal{G}^i$ is identifiable. As our model defines a distribution over graphs, its predictions are meaningful even when the amount of data is insufficient for identifiability: in this case, the model would sample graphs that are compatible with the given data. Empirically, we found that our model can make reasonable predictions even with a small amount of samples per intervention and improves as more samples are observed (Section 6.4).

Graph distribution. We specified a distribution over $\mathcal{G}$ in terms of the number of nodes N (graph size) and number of edges (graph density) present in $\mathcal{G}$. As shown in Zheng et al. (2018); Yu et al. (2019); Ke et al. (2020a), larger and denser graphs are more challenging to learn. We varied N from 5 to 80. We used the Erdős–Rényi (ER) metric to vary density and evaluated our model on ER-1 and ER-2 graphs, as in Yu et al. (2019); Brouillard et al. (2020); Scherrer et al. (2021). We generated an adjacency matrix A by first sampling a lower-triangular matrix to ensure that it represents a DAG, and by then permuting the order of the nodes to ensure random ordering.

Conditional probability distributions. We performed ancestral sampling on the underlying CBN. We considered both continuous and discrete nodes. For continuous nodes, we generated *continuous data* using three different methods following similar setups in previous works: (i) linear models (*linear data*) (Zheng et al., 2018; Yu et al., 2019), (ii) nonlinear with additive noise models (*ANM data*) (Brouillard et al., 2020; Lippe et al., 2021), and (iii) nonlinear with non-additive noise models using neural networks *(NN data)* (Brouillard et al., 2020; Lippe et al., 2021). For discrete nodes, we generated discrete data using two different methods: MLP (*MLP data*) and Dirichlet (*Dirichlet data*) conditional-probability table generators. Following past work (Ke et al., 2020a; Scherrer et al., 2021), we used a randomly initialized network. The Dirichlet generator filled in the rows of a conditional probability table by sampling a categorical distribution from a Dirichlet prior with symmetric parameters α. (We remind the reader that this generative procedure is performed prior to node ordering being randomized for presentation to the learning model.) For more details, please refer to Appendix A.2.

5 RELATED WORK

Methods for inferring causal graphs can broadly be categorized into score-based (continuous optimization methods included), constraint-based, and asymmetry-based methods. Score-based methods search through the space of possible candidate graphs, usually DAGs, and ranks them based on some scoring function (Chickering, 2002; Cooper & Yoo, 1999; Goudet et al., 2017; Hauser & Bühlmann, 2012; Heckerman et al., 1995; Tsamardinos et al., 2006; Huang et al., 2018; Zhu & Chen, 2019). Recently, Zheng et al. (2018); Yu et al. (2019); Lachapelle et al. (2019) framed the structure search as

a continuous optimization problem. There also exist score-based methods that use a mix of continuous and discrete optimization (Bengio et al., 2019; Ke et al., 2020a; Lippe et al., 2021; Scherrer et al., 2021). Constraint-based methods (Monti et al., 2019; Spirtes et al., 2000; Sun et al., 2007; Zhang et al., 2012; Zhu & Chen, 2019) infer the DAG by analyzing conditional independencies in the data. Eaton & Murphy (2007) use dynamic programming techniques. Asymmetry-based methods (Shimizu et al., 2006; Hoyer et al., 2009; Peters et al., 2011; Daniusis et al., 2012; Budhathoki & Vreeken, 2017; Mitrovic et al., 2018) assume asymmetry between cause and effect in the data and use this to estimate the causal structure. Peters et al. (2016); Ghassami et al. (2017); Rojas-Carulla et al. (2018); Heinze-Deml et al. (2018a) exploit invariance across environments to infer causal structure. Mooij et al. (2016) propose a modelling framework that leverages existing methods.

Several learning-based methods have been proposed (Bengio et al., 2019; Goudet et al., 2018; Guyon, 2013; 2014; Kalainathan et al., 2018; Ke et al., 2020a;b; Lachapelle et al., 2022; Lopez-Paz et al., 2015b; Wang et al., 2021b; Zhu & Chen, 2019). These works are mainly concerned with learning only part of the causal induction pipeline, such as the scoring function, and hence are significantly different from our work, which uses an end-to-end supervised learning approach to learn to map from datasets to graphs. Neural network methods equipped with learned masks exist in the literature (Douglas et al., 2017; Goyal et al., 2021; Ivanov et al., 2018; Li et al., 2019; Yoon et al., 2018), but only a few have been adapted to causal inference. Several transformer models Goyal et al. (2022); Kossen et al. (2021); Müller et al. (2021) have been proposed for learning to map from datasets to targets. However, none have been applied to causal discovery, although Löwe et al. (2022) proposes a neural-network based approach for causal discovery on time-series data. A few supervised learning approaches have been proposed either framing the task as a kernel mean embedding classification problem (Lopez-Paz et al., 2015a;b) or operating directly on covariance matrices (Li et al., 2020) or binary classification problem of identifying v-structures (Dai et al., 2021). These models accept observational data only (see Table 1), and because causal identifiability requires *both observational and interventional* data, our model is in principle more powerful.

Data Type	**RCC**	**DAG-EQ**	**CSIvA**
Observational	✓	✓	✓
Interventional	X	X	✓
Linear dependencies	✓	✓	✓
Non-linear dependencies	✓	X	✓

Table 1: Data-type comparison between CSIvA and other supervised approaches to causal structure induction (RCC (Lopez-Paz et al., 2015a;b) and DAG-EQ (Li et al., 2020)).

6 EXPERIMENTS

We report on a series of experiments of increasing challenge to our supervised approach to causal structure induction. First, we examined whether CSIvA generalizes well on synthetic data for which the training and test distributions are identical (Section 6.1). This experiment tests whether the model can learn to map from a dataset to a structure. Second, we examined generalization to an out-of-distribution (OOD) test distribution, and we determined hyperparameters of the synthetic data generating process that are most robust to OOD testing (Section 6.2). Third, we trained CSIvA using the hyperparameters from our second experiment and evaluated it on a different type of OOD test distribution from several naturalistic CBNs (Section 6.3). This experiment is the most important test of our hypothesis that causal structure of synthetic datasets can be a useful proxy for discovering causal structure in realistic settings. Lastly, we performed a set of ablation studies to analyze the performance of CSIvA under different settings (Section 6.4). Please refer to Appendix A.3 for details on the hyperparameters.

Comparisons to baselines. We compared CSIvA to a range of methods considered to be state-of-the-art in the literature, ranging from classic to neural-network based causal discovery baselines. For both in-distribution and OOD experiments, we compare to 4 very strong baselines: DAG-GNN (Yu et al., 2019), non-linear ICP (Heinze-Deml et al., 2018b), DCDI (Brouillard et al., 2020), and ENCO (Lippe et al., 2021). For OOD experiments to naturalistic graphs, we compare to 5 additional baselines (Chickering, 2002; Hauser & Bühlmann, 2012; Zheng et al., 2018; Gamella & Heinze-Deml, 2020; Li et al., 2020). Because some methods use only observational data and others do not scale well to large N, we could not compare to all methods in all experiments. See Appendix A.4 for further discussion of alternative methods and conditions under which they can be used.

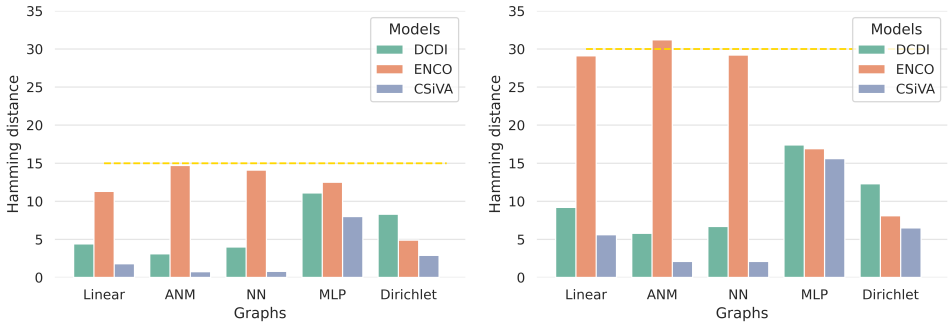

(a) Results on $N = 30$ and ER-1 graphs. (b) Results on $N = 30$ and ER-2 graphs.

Figure 3: Hamming distance $\mathcal{H}$ between predicted and ground-truth adjacency matrices on 5 different data types: Linear, ANM, NN, MLP and Dirichlet data, compared to DCDI (Brouillard et al., 2020) and ENCO (Lippe et al., 2021) on $N = 30$ graphs, averaged over 128 sampled graphs. The dotted line indicates the value of the all-absent baseline. CSIvA significantly outperforms all other baselines for all data types.

6.1 In-distribution experiments

We begin by investigating whether CSIvA can learn to map from data to structures in the case in which the training and test distributions are identical. In this setting, our supervised approach has an advantage over unsupervised ones, as it can learn about the training distribution and leverage this knowledge during testing. We evaluate CSIvA for $N \leq 80$ graphs. We examined the performance on data with increasing order of difficulty, starting with linear (continuous data), before moving to non-linear cases (ANM, NN, MLP and Dirichlet data). See Fig. 3 for comparisons between CSIvA and strong baselines on all data types ($N = 30$), showing that CSIvA significantly outperforms baselines for a wide range of data types. For all but the Dirichlet data, we summarize the high-level results here, but detailed results and plots for all experiments can be found in Appendix A.5.

Linear data. Results on continuous linear data for $N \leq 20$ and $30 \leq N \leq 80$ are presented in Tables 4 and 5 in the Appendix. CSIvA outperforms non-linear ICP, DAG-GNN, DCDI and ENCO. The difference in performance increases with N.

ANM data. Results on continuous ANM data for $N \leq 80$ are presented in Table 6 in the Appendix. CSIvA significantly outperforms the strongest baselines: DCDI and ENCO. Again, the difference in performance increases with N.

NN data. Results on continuous NN data are reported in Table 7 in the Appendix. CSIvA significantly outperforms strongest baselines: DCDI and ENCO, with improved benefit for larger N.

MLP data. Results on MLP data are shown in Fig. 5(b) in the Appendix. CSIvA significantly outperforms non-linear ICP, DAG-GNN, DCDI and ENCO. Differences become more apparent with larger graph sizes ($N \geq 10$) and denser graphs (ER-2 vs ER-1).

Dirichlet data. The Dirichlet data requires setting the values of the parameter α. Hence, we run two sets of experiments on this data. In the first set of experiments, we investigated how different values of α impact learning in CSIvA. As shown in Table 11 in the appendix, CSIvA performs well on all data with $\alpha \leq 0.5$, achieving $\mathcal{H} < 2.5$ in all cases. CSIvA still performs well when $\alpha = 1.0$, achieving $\mathcal{H} < 5$ on size 10 graphs. Learning with $\alpha > 1$ is more challenging. This is not surprising, as $\alpha > 1$ tends to generate more uniform distributions, which are not informative of the causal relationship between nodes.

In the second set of experiments, we compared CSIvA to DCDI and ENCO, as they are the strongest performing baselines. We run the comparisons on graphs of size up to $N \leq 80$. To limit the number of experiments to run, we set $\alpha = 0.1$, as this allows the conditional probabilities to concentrate on non-uniform distributions, which is more likely to be true in realistic settings. As shown in Fig. 4, our model significantly outperforms DCDI and ENCO on all graphs (up to $N \leq 80$). As with other data types, the difference becomes more apparent as the size of the graphs grows ($N \geq 50$), as larger graphs are more challenging to learn.

Soft interventions and unknown interventions. We additionally evaluated CSIvA on soft interventions, and on hard interventions for which the model did not know the intervention node (*unknown interventions*). In both cases, we focus on Dirichlet data with $\alpha = 0.1$ and $\alpha = 0.25$ for ER-1 and ER-2 graphs of size $N \leq 20$. Results for the performance of CSIvA on soft interventions are shown in Table 13 in the Appendix. CSIvA performed well on all graphs, achieving hamming distance $\mathcal{H} < 5$ on all graphs. For details about the data generation process, refer to Appendix Section A.5.6.

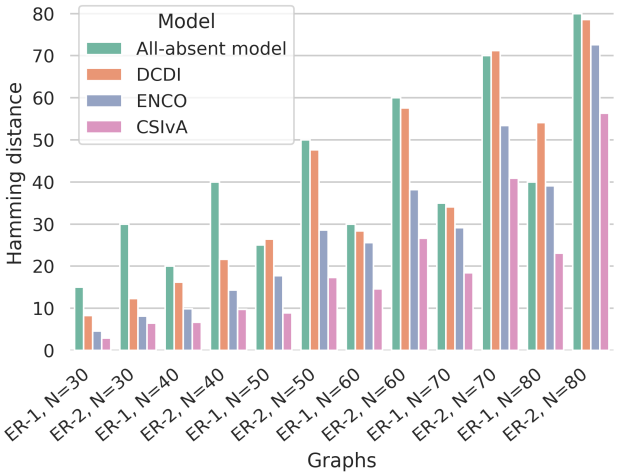

Figure 4: **Results on Dirichlet data for** $30 \leq N \leq 80$. Hamming distance $\mathcal{H}$ between predicted and ground-truth adjacency matrices, averaged over 128 sampled graphs. CSIvA significantly outperforms DCDI and ENCO, both of which are very strong baselines. The difference in performance increases with N.

Results for the performance of CSIvA on unknown interventions are shown in Appendix Table 14. CSIvA achieves strong performance on all graphs, with hamming distance $\mathcal{H} < 7$ on all graphs. Note that CSIvA loses almost no performance despite not knowing the intervention; the biggest difference in hamming distance between known and unknown interventions on all graphs is $\mathcal{H} < 1.0$. For more details, refer to Section A.5.7 in the Appendix.

6.2 Out-of-distribution experiments

In this set of experiments, we evaluated CSIvA's ability to generalize with respect to aspects of the data generating distribution that are often unknown, namely graph density and parameters of the CPDs, such as the α values of the Dirichlet distribution.

Varying graph density. We evaluated how well our model performs when trained and tested on CBNs with varying graph density on MLP and $\alpha = 1$ Dirichlet data. We fixed the number of nodes to $N = 7$, with variables able to take on discrete values in $\{1, 2, 3\}$. The graphs in training and test datasets can take ER degree $\in \{1, 2, 3\}$. Results are shown in Table 15 in the appendix for the MLP data and Table 16 in the appendix for the Dirichlet data. For the MLP data, models trained on ER-2 graph generalizes the best. For Dirichlet data, there isn't one value of graph density that consistently generalizes best across graphs with different densities. Nevertheless, ER-2 graphs give a balanced trade-off and generalizes well across graphs with different sparsity.

Varying α. We next trained and evaluated on data generated from Dirichlet distributions with $\alpha \in \{0.1, 0.25, 0.5\}$. Results for ER-1 graphs with $N = 7$ are found in Table 17. There isn't a value of α that performs consistently well across different values of α for the test data. Nevertheless, $\alpha = 0.25$ is a balanced trade-off and generalizes well across test data with $0.1 \leq \alpha \leq 0.5$.

6.3 Sim-to-real experiments

In this final set of experiments, we evaluated CSIvA's ability to generalize from being trained on MLP and Dirichlet data to being evaluated on the widely used Sachs (Sachs et al., 2005), Asia (Lauritzen & Spiegelhalter, 1988) and Child (Spiegelhalter & Cowell, 1992) CBNs from the BnLearn repository, which have $N = 11$, $N = 8$ and $N = 20$ nodes respectively. We followed the established protocol from Ke et al. (2020a); Lippe et al. (2021); Scherrer et al. (2021) of sampling observational and interventional data from the CBNs provided by the repository. These experiments are the most important test of our hypothesis that causal structure of synthetic datasets can be a useful proxy for discovering causal structure in realistic settings.

We emphasize that all hyperparameters for the MLP and Dirichlet data and for the learning procedure were chosen *a priori*; only after the architecture and parameters were finalized was the model tested

on these benchmarks. Furthermore, to keep the setup simple, we trained on data sampled from a single set of hyperparameters instead of a broader mixture. Findings in Section 6.2 suggest that ER-2 graphs with $\alpha = 0.25$ work well overall and hence were chosen. Results are reported in Table 2, comparing to a range of baselines from Squires et al. (2020); Heinze-Deml et al. (2018b); Yu et al. (2019); Gamella & Heinze-Deml (2020); Brouillard et al. (2020); Lippe et al. (2021) and others.

CSIvA trained on both MLP and Dirichlet data significantly outperforms all other methods on both the Asia and Sachs datasets. This serves as strong evidence that our model can learn to induce causal structures in the more realistic real-world CBNs, while only trained on synthetic data.

	Asia	**Sachs**	**Child**
Number of nodes	8	11	20
All-absent Baseline	8	17	25
GES Chickering (2002)	4	19	33
DAG-notears Zheng et al. (2018)	14	22	23
DAG-GNN Yu et al. (2019)	8	13	20
GES Hauser & Bühlmann (2012)	11	16	31
ICP Peters et al. (2016)	8	17	27*
Non-linear ICP Heinze-Deml et al. (2018b)	8	16	23*
DAG-EQ Li et al. (2020)	-	16	-
DCDI-DSF Brouillard et al. (2020)	7	33	18
ENCO Lippe et al. (2021)	5	9	14
CSIvA (MLP data)	**3**	**6**	**11**
CSIvA (Dirichlet data)	**3**	**5**	**10**

Table 2: **Results on Asia, Sachs and Child data:** Hamming distance $\mathcal{H}$ between predicted and ground-truth adjacency matrices. *To maintain computational tractability, the number of parents was limited to 3.

6.4 Detailed analyses

In order to better understand model performance, and which model components were most critical, we performed further analyses. We describe here a subset of the studies performed; please refer to Appendix A.7 for the full results, including ablations.

Acyclicity. We analyzed the generated (sampled) graphs for acyclicity. We evaluated using Dirichlet data with $\alpha = 0.1$ and $\alpha = 0.25$ on ER-1 and ER-2 graphs of size $N \leq 20$. For each setting, we evaluated the proposed model on 128 random graphs, and we found that none of the generated graphs contains any cycles, i.e., all generated graphs are acyclic.

Visualization of generated graphs. We visualized some of the generated graphs in Figure 8 and Figure 9 in the Appendix. Note that samples are randomly drawn, and all are acyclic.

Identifiability upon seeing intervention data. Here, we investigate how varying the proportion of interventional data impacts the performance of the proposed model. As shown in Figure 7 (Appendix), the model's performance improves (Hamming distance decreases) almost monotonically as the amount of interventional data increases, from $0 - 100\%$. This is a clear indication that our model is able to extract information from interventional data for identifying the graph structure. For more details on the results and the how the experiments are conducted, please refer to Section A.7.3.

Ablation studies. We investigate the role of various components in CSIvA. For example, what is the effect of having the auxiliary loss or the sample-level attention. We found that all the different components play an important role in our model. For details, see Appendix A.7.

7 Discussion

In this paper, we have presented a novel approach towards causal graph structure inference. Our method is based on learning from synthetic data in order to obtain a strong learning signal (in the form of explicit supervision), using a novel transformer-based architecture which directly analyzes the data and computes a distribution of candidate graphs. Through a comprehensive and detailed set of experiments, we demonstrated that even though only trained on synthetic data, our model generalizes to out-of-distribution datasets, and robustly outperforms comparison methods under a wide range of conditions. A direction of future work would be to use the proposed framework for learning causal structure from raw visual data. This could be useful, e.g. in an RL setting in which an RL agent interacts with the environment via observing low level pixel data (Ahmed et al., 2020; Ke et al., 2021; Wang et al., 2021a).

REFERENCES

Ossama Ahmed, Frederik Träuble, Anirudh Goyal, Alexander Neitz, Yoshua Bengio, Bernhard Schölkopf, Manuel Wüthrich, and Stefan Bauer. Causalworld: A robotic manipulation benchmark for causal structure and transfer learning. *arXiv preprint arXiv:2010.04296*, 2020.

Jimmy Lei Ba, Jamie Ryan Kiros, and Geoffrey E Hinton. Layer normalization. *arXiv preprint arXiv:1607.06450*, 2016.

Yoshua Bengio, Tristan Deleu, Nasim Rahaman, Rosemary Ke, Sébastien Lachapelle, Olexa Bilaniuk, Anirudh Goyal, and Christopher Pal. A meta-transfer objective for learning to disentangle causal mechanisms. *arXiv preprint arXiv:1901.10912*, 2019.

Philippe Brouillard, Sébastien Lachapelle, Alexandre Lacoste, Simon Lacoste-Julien, and Alexandre Drouin. Differentiable causal discovery from interventional data. *Advances in Neural Information Processing Systems*, 33:21865–21877, 2020.

Kailash Budhathoki and Jilles Vreeken. Causal inference by stochastic complexity. *arXiv:1702.06776*, 2017.

Federico Castelletti and Alessandro Mascaro. Bcdag: An r package for bayesian structure and causal learning of gaussian dags. *arXiv preprint arXiv:2201.12003*, 2022.

David Maxwell Chickering. Optimal structure identification with greedy search. *Journal of machine learning research*, 3(Nov):507–554, 2002.

Gregory F. Cooper and Changwon Yoo. Causal Discovery from a Mixture of Experimental and Observational Data. In *Proceedings of the Fifteenth Conference on Uncertainty in Artificial Intelligence*, UAI'99, pp. 116–125, San Francisco, CA, USA, 1999.

Haoyue Dai, Rui Ding, Yuanyuan Jiang, Shi Han, and Dongmei Zhang. Ml4c: Seeing causality through latent vicinity. *arXiv preprint arXiv:2110.00637*, 2021.

Povilas Daniusis, Dominik Janzing, Joris Mooij, Jakob Zscheischler, Bastian Steudel, Kun Zhang, and Bernhard Schölkopf. Inferring deterministic causal relations. *arXiv preprint arXiv:1203.3475*, 2012.

Jacob Devlin, Ming-Wei Chang, Kenton Lee, and Kristina Toutanova. Bert: Pre-training of deep bidirectional transformers for language understanding. *arXiv preprint arXiv:1810.04805*, 2018.

Laura Douglas, Iliyan Zarov, Konstantinos Gourgoulias, Chris Lucas, Chris Hart, Adam Baker, Maneesh Sahani, Yura Perov, and Saurabh Johri. A universal marginalizer for amortized inference in generative models. *arXiv preprint arXiv:1711.00695*, 2017.

Mathias Drton and Marloes H. Maathuis. Structure learning in graphical modeling. *Annual Review of Statistics and Its Application*, 4(1):365–393, 2017.

Daniel Eaton and Kevin Murphy. Bayesian structure learning using dynamic programming and MCMC. In *Uncertainty in Artificial Intelligence*, pp. 101–108, 2007.

Frederick Eberhardt, Clark Glymour, and Richard Scheines. N-1 experiments suffice to determine the causal relations among n variables. In *Innovations in machine learning*, pp. 97–112. Springer, 2006.

Juan L Gamella and Christina Heinze-Deml. Active invariant causal prediction: Experiment selection through stability. *arXiv preprint arXiv:2006.05690*, 2020.

AmirEmad Ghassami, Saber Salehkaleybar, Negar Kiyavash, and Kun Zhang. Learning causal structures using regression invariance. In *Advances in Neural Information Processing Systems*, pp. 3011–3021, 2017.

Clark Glymour, Kun Zhang, and Peter Spirtes. Review of causal discovery methods based on graphical models. *Frontiers in Genetics*, 10:524, 2019.

Olivier Goudet, Diviyan Kalainathan, Philippe Caillou, Isabelle Guyon, David Lopez-Paz, and Michèle Sebag. Causal generative neural networks. *arXiv preprint arXiv:1711.08936*, 2017.

Olivier Goudet, Diviyan Kalainathan, Philippe Caillou, Isabelle Guyon, David Lopez-Paz, and Michele Sebag. Learning functional causal models with generative neural networks. In *Explainable and Interpretable Models in Computer Vision and Machine Learning*, pp. 39–80. Springer, 2018.

Anirudh Goyal, Aniket Didolkar, Nan Rosemary Ke, Charles Blundell, Philippe Beaudoin, Nicolas Heess, Michael C Mozer, and Yoshua Bengio. Neural production systems. *Advances in Neural Information Processing Systems*, 34, 2021.

Anirudh Goyal, Abram L Friesen, Andrea Banino, Theophane Weber, Nan Rosemary Ke, Adria Puigdomenech Badia, Arthur Guez, Mehdi Mirza, Ksenia Konyushkova, Michal Valko, et al. Retrieval-augmented reinforcement learning. *arXiv preprint arXiv:2202.08417*, 2022.

Isabelle Guyon. Cause-effect pairs kaggle competition, 2013. *URL https://www. kaggle. com/c/cause-effect-pairs*, pp. 165, 2013.

Isabelle Guyon. Chalearn fast causation coefficient challenge, 2014. *URL https://www. codalab. org/competitions/1381*, pp. 165, 2014.

Alain Hauser and Peter Bühlmann. Characterization and greedy learning of interventional markov equivalence classes of directed acyclic graphs. *The Journal of Machine Learning Research*, 13(1): 2409–2464, 2012.

Kaiming He, Xiangyu Zhang, Shaoqing Ren, and Jian Sun. Deep residual learning for image recognition. In *Proceedings of the IEEE conference on computer vision and pattern recognition*, pp. 770–778, 2016.

David Heckerman, Dan Geiger, and David M Chickering. Learning bayesian networks: The combination of knowledge and statistical data. *Machine learning*, 20(3):197–243, 1995.

Christina Heinze-Deml, Marloes H Maathuis, and Nicolai Meinshausen. Causal structure learning. *Annual Review of Statistics and Its Application*, 5:371–391, 2018a.

Christina Heinze-Deml, Jonas Peters, and Nicolai Meinshausen. Invariant causal prediction for nonlinear models. *Journal of Causal Inference*, 6(2), 2018b.

Patrik O Hoyer, Dominik Janzing, Joris M Mooij, Jonas Peters, and Bernhard Schölkopf. Nonlinear causal discovery with additive noise models. In *Advances in neural information processing systems*, pp. 689–696, 2009.

Biwei Huang, Kun Zhang, Yizhu Lin, Bernhard Schölkopf, and Clark Glymour. Generalized score functions for causal discovery. In *Proceedings of the 24th ACM SIGKDD international conference on knowledge discovery & data mining*, pp. 1551–1560, 2018.

Oleg Ivanov, Michael Figurnov, and Dmitry Vetrov. Variational autoencoder with arbitrary conditioning. *arXiv preprint arXiv:1806.02382*, 2018.

Diviyan Kalainathan, Olivier Goudet, Isabelle Guyon, David Lopez-Paz, and Michèle Sebag. Sam: Structural agnostic model, causal discovery and penalized adversarial learning. *arXiv preprint arXiv:1803.04929*, 2018.

Nan Rosemary Ke, Olexa Bilaniuk, Anirudh Goyal, Stefan Bauer, Bernhard Schölkopf, Michael Curtis Mozer, Hugo Larochelle, Christopher Pal, and Yoshua Bengio. Dependency structure discovery from interventions. 2020a.

Nan Rosemary Ke, Jane Wang, Jovana Mitrovic, Martin Szummer, Danilo J Rezende, et al. Amortized learning of neural causal representations. *arXiv preprint arXiv:2008.09301*, 2020b.

Nan Rosemary Ke, Aniket Rajiv Didolkar, Sarthak Mittal, Anirudh Goyal, Guillaume Lajoie, Stefan Bauer, Danilo Jimenez Rezende, Michael Curtis Mozer, Yoshua Bengio, and Christopher Pal. Systematic evaluation of causal discovery in visual model based reinforcement learning. 2021.

Diederik P Kingma and Jimmy Ba. Adam: A method for stochastic optimization. *arXiv preprint arXiv:1412.6980*, 2014.

Daphne Koller and Nir Friedman. *Probabilistic Graphical Models: Principles and Techniques*. MIT Press, 2009.

Timo Koski and John Noble. A review of Bayesian networks and structure learning. *Mathematica Applicanda*, 40, 2012.

Jannik Kossen, Neil Band, Clare Lyle, Aidan N Gomez, Thomas Rainforth, and Yarin Gal. Self-attention between datapoints: Going beyond individual input-output pairs in deep learning. *Advances in Neural Information Processing Systems*, 34, 2021.

Sébastien Lachapelle, Philippe Brouillard, Tristan Deleu, and Simon Lacoste-Julien. Gradient-based neural dag learning. *arXiv preprint arXiv:1906.02226*, 2019.

Sébastien Lachapelle, Pau Rodriguez, Yash Sharma, Katie E Everett, Rémi Le Priol, Alexandre Lacoste, and Simon Lacoste-Julien. Disentanglement via mechanism sparsity regularization: A new principle for nonlinear ica. In *Conference on Causal Learning and Reasoning*, pp. 428–484. PMLR, 2022.

Steffen L Lauritzen and David J Spiegelhalter. Local computations with probabilities on graphical structures and their application to expert systems. *Journal of the Royal Statistical Society: Series B (Methodological)*, 50(2):157–194, 1988.

Hebi Li, Qi Xiao, and Jin Tian. Supervised whole dag causal discovery. *arXiv preprint arXiv:2006.04697*, 2020.

Yang Li, Shoaib Akbar, and Junier B Oliva. Flow models for arbitrary conditional likelihoods. *arXiv preprint arXiv=1909.06319*, 2019.

Yujia Li, David Choi, Junyoung Chung, Nate Kushman, Julian Schrittwieser, Rémi Leblond, Tom Eccles, James Keeling, Felix Gimeno, Agustin Dal Lago, Thomas Hubert, Peter Choy, Cyprien de Masson d'Autume, Igor Babuschkin, Xinyun Chen, Po-Sen Huang, Johannes Welbl, Sven Gowal, Alexey Cherepanov, James Molloy, Daniel J. Mankowitz, Esme Sutherland Robson, Pushmeet Kohli, Nando de Freitas, Koray Kavukcuoglu, and Oriol Vinyals. Competition-level code generation with alphacode. *arXiv preprint arXiv:2203.07814*, 2022.

Phillip Lippe, Taco Cohen, and Efstratios Gavves. Efficient neural causal discovery without acyclicity constraints. *arXiv preprint arXiv:2107.10483*, 2021.

David Lopez-Paz, Krikamol Muandet, and Benjamin Recht. The randomized causation coefficient. *J. Mach. Learn. Res.*, 16:2901–2907, 2015a.

David Lopez-Paz, Krikamol Muandet, Bernhard Schölkopf, and Iliya Tolstikhin. Towards a learning theory of cause-effect inference. In *International Conference on Machine Learning*, pp. 1452–1461, 2015b.

Sindy Löwe, David Madras, Richard Zemel, and Max Welling. Amortized causal discovery: Learning to infer causal graphs from time-series data. In *Conference on Causal Learning and Reasoning*, pp. 509–525. PMLR, 2022.

Ahmed Mabrouk, Christophe Gonzales, Karine Jabet-Chevalier, and Eric Chojnacki. An efficient Bayesian network structure learning algorithm in the presence of deterministic relations. *Frontiers in Artificial Intelligence and Applications*, 263:567–572, 2014.

Jovana Mitrovic, Dino Sejdinovic, and Yee Whye Teh. Causal inference via kernel deviance measures. In *Advances in Neural Information Processing Systems*, pp. 6986–6994, 2018.

Ricardo Pio Monti, Kun Zhang, and Aapo Hyvarinen. Causal discovery with general non-linear relationships using non-linear ica. *arXiv preprint arXiv:1904.09096*, 2019.

Joris M Mooij, Sara Magliacane, and Tom Claassen. Joint causal inference from multiple contexts. *arXiv preprint arXiv:1611.10351*, 2016.

Samuel Müller, Noah Hollmann, Sebastian Pineda Arango, Josif Grabocka, and Frank Hutter. Transformers can do bayesian inference. *arXiv preprint arXiv:2112.10510*, 2021.

Judea Pearl. *Causality*. Cambridge university press, 2009.

J. Peters, J. M. Mooij, D. Janzing, and B. Schölkopf. Identifiability of causal graphs using functional models. In *Proceedings of the 27th Annual Conference on Uncertainty in Artificial Intelligence (UAI)*, pp. 589–598, 2011.

Jonas Peters, Peter Bühlmann, and Nicolai Meinshausen. Causal inference by using invariant prediction: identification and confidence intervals. *Journal of the Royal Statistical Society: Series B (Statistical Methodology)*, 78(5):947–1012, 2016.

Mateo Rojas-Carulla, Bernhard Schölkopf, Richard Turner, and Jonas Peters. Invariant models for causal transfer learning. *The Journal of Machine Learning Research*, 19(1):1309–1342, 2018.

Karen Sachs, Omar Perez, Dana Pe'er, Douglas A Lauffenburger, and Garry P Nolan. Causal protein-signaling networks derived from multiparameter single-cell data. *Science*, 308(5721):523–529, 2005.

Nino Scherrer, Olexa Bilaniuk, Yashas Annadani, Anirudh Goyal, Patrick Schwab, Bernhard Schölkopf, Michael C Mozer, Yoshua Bengio, Stefan Bauer, and Nan Rosemary Ke. Learning neural causal models with active interventions. *arXiv preprint arXiv:2109.02429*, 2021.

Shohei Shimizu, Patrik O Hoyer, Aapo Hyvärinen, and Antti Kerminen. A linear non-gaussian acyclic model for causal discovery. *Journal of Machine Learning Research*, 7(Oct):2003–2030, 2006.

D. J. Spiegelhalter and R. G. Cowell. Learning in probabilistic expert systems. *Bayesian Statistics*, 4: 447–466, 1992.

Peter Spirtes, Clark N Glymour, Richard Scheines, David Heckerman, Christopher Meek, Gregory Cooper, and Thomas Richardson. *Causation, prediction, and search*. MIT press, 2000.

Chandler Squires, Yuhao Wang, and Caroline Uhler. Permutation-based causal structure learning with unknown intervention targets. In *Conference on Uncertainty in Artificial Intelligence*, pp. 1039–1048. PMLR, 2020.

Xiaohai Sun, Dominik Janzing, Bernhard Schölkopf, and Kenji Fukumizu. A kernel-based causal learning algorithm. In *Proceedings of the 24th international conference on Machine learning*, pp. 855–862. ACM, 2007.

Ioannis Tsamardinos, Laura E Brown, and Constantin F Aliferis. The max-min hill-climbing bayesian network structure learning algorithm. *Machine learning*, 65(1):31–78, 2006.

Ashish Vaswani, Noam Shazeer, Niki Parmar, Jakob Uszkoreit, Llion Jones, Aidan N Gomez, Łukasz Kaiser, and Illia Polosukhin. Attention is all you need. In *Advances in neural information processing systems*, pp. 5998–6008, 2017.

Jane X Wang, Michael King, Nicolas Porcel, Zeb Kurth-Nelson, Tina Zhu, Charlie Deck, Peter Choy, Mary Cassin, Malcolm Reynolds, Francis Song, et al. Alchemy: A structured task distribution for meta-reinforcement learning. *arXiv preprint arXiv:2102.02926*, 2021a.

Xiaoqiang Wang, Yali Du, Shengyu Zhu, Liangjun Ke, Zhitang Chen, Jianye Hao, and Jun Wang. Ordering-based causal discovery with reinforcement learning. *arXiv preprint arXiv:2105.06631*, 2021b.

Jinsung Yoon, James Jordon, and Mihaela Van Der Schaar. Gain: Missing data imputation using generative adversarial nets. *arXiv preprint arXiv:1806.02920*, 2018.

Yue Yu, Jie Chen, Tian Gao, and Mo Yu. Dag-gnn: Dag structure learning with graph neural networks. *arXiv preprint arXiv:1904.10098*, 2019.

Kun Zhang, Jonas Peters, Dominik Janzing, and Bernhard Schölkopf. Kernel-based conditional independence test and application in causal discovery. *arXiv preprint arXiv:1202.3775*, 2012.

Xun Zheng, Bryon Aragam, Pradeep K Ravikumar, and Eric P Xing. DAGs with NO TEARS: Continuous optimization for structure learning. In *Advances in Neural Information Processing Systems*, pp. 9472–9483, 2018.

Shengyu Zhu and Zhitang Chen. Causal discovery with reinforcement learning. *arXiv preprint arXiv:1906.04477*, 2019.

A APPENDIX

CONTENTS

A.1 Transformer Neural Networks 16
A.2 Synthetic Data 16
A.3 Hyperparameters 17
A.4 Comparisons to Baselines 18
A.5 Detailed results for Section 6.1 18
A.5.1 Results on linear data 18
A.5.2 Results on ANM data 18
A.5.3 Results on NN data 19
A.5.4 Results on MLP data 19
A.5.5 Results on Dirichlet data. 19
A.5.6 Soft interventions 20
A.5.7 Unknown Interventions 21
A.6 Detailed results for Out-of-distribution experiments 22
A.7 Ablation studies and analyses 22
A.7.1 Visualization of sampled graphs 22
A.7.2 Acyclicity of generated graphs 23
A.7.3 Identifiability upon seeing intervention data. 25
A.7.4 Varying number of samples 26
A.7.5 Ablation studies 26

A.1 TRANSFORMER NEURAL NETWORKS

The transformer architecture, introduced in Vaswani et al. (2017), is a multi-layer neural network architecture using stacked self-attention and point-wise, fully connected, layers. The classic transformer architecture has an encoder and a decoder, but the encoder and decoder do not necessarily have to be used together.

Scaled dot-product attention. The attention mechanism lies at the core of the transformer architecture. The transformer architecture uses a special form of attention, called the scaled dot-product attention. The attention mechanism allows the model to flexibility learn to weigh the inputs depending on the context. The input to the QKV attention consists of a set of queries, keys and value vectors. The queries and keys have the same dimensionality of d_k, and values often have a different dimensionality of d_v. Transformers compute the dot products of the query with all keys, divide each by $\sqrt{d_k}$, and apply a softmax function to obtain the weights on the values. In practice, transformers compute the attention function on a set of queries simultaneously, packed together into a matrix Q. The keys and values are also packed together into matrices K and V. The matrix of outputs is computed as: $\text{Attention}(Q, K, V) = \text{softmax}(\frac{QK^T}{\sqrt{d_k}})V$.

Encoder. The encoder is responsible for processing and summarizing the information in the inputs. The encoder is composed of a stack of N identical layers, where each layer has two sub-layers. The first sub-layer consists of a multi-head self-attention mechanism, and the second is a simple, position-wise fully connected feed-forward network. Transformers employ a residual connection (He et al., 2016) around each of the two sub-layers, followed by layer normalization Ba et al. (2016). That is, the output of each sub-layer is $\text{LayerNorm}(x + \text{Sublayer}(x))$, where $\text{Sublayer}(x)$ is the function implemented by the sub-layer itself.

Decoder. The decoder is responsible for transforming the information summarized by the encoder into the outputs. The decoder also composes of a stack of N identical layers, with a small difference in the decoder transformer layer. In addition to the two sub-layers in each encoder layer, a decoder layer consists of a third sub-layer. The third sub-layer performs a multi-head attention over the output of the encoder stack. Similar to the encoder, transformers employ residual connections around each of the sub-layers, followed by layer normalization. Transformers also modify the self-attention sub-layer in the decoder stack to prevent positions from attending to subsequent positions. This masking, combined with fact that the output embeddings are offset by one position, ensures that the predictions for position i can depend only on the known outputs at positions less than i.

A.2 SYNTHETIC DATA

In Section 4, we introduced the types of methods used to generate the conditional probability distribution. In this section, we discuss the details of these methods.

We evaluate our model on datasets generated from 5 different methods, which covers both continuous and discrete valued data generated with a varying degree of difficulty. For continuous data, we generated the data using three different methods: *linear*, *non-linear additive noise model* (ANM) and *non-linear non-additive noise neural network model* (NN). For discrete data, we generated data using two different methods: *MLP* and *Dirichlet*. Let X be a $N \times S$ matrix representing S samples of a CBN with N nodes and weighted adjacency matrix A, and let Z be a random matrix of elements in $\mathcal{N}(0, 0.1)$. We describe each type of how different types of data is generated.

- For *linear data*, we follow the setup in Zheng et al. (2018) and Yu et al. (2019). Specifically, we generated data as $X_{n,:} = A_{n,:}X + Z_{n,:}$. The biases were initialized using $U[-0.5, 0.5]$, and the individual weights were initialized using a truncated normal distribution with standard deviation of 1.5. For nodes with interventions, values are sampled from the uniform distribution $U[-1, 1]$.
- For *additive noise models (ANM)* , we follow the setup in (Brouillard et al., 2020; Lippe et al., 2021). We generated the data as $X_{n,:} = F_{n,:}(X) + 0.4 \cdot Z_{n,:}$, where F is fully connected neural network, the weights are randomly initialized from $\mathcal{N}(0, 1)$. The neural network has one hidden layer with 10 hidden units, the activation function is a leaky relu

with a slop of 0.25. The noise variables are sampled from $\mathcal{N}(0, \sigma^2)$, where $\sigma^2 \sim \mathcal{U}[1, 2]$. For nodes with interventions, values are sampled from the uniform distribution $\mathcal{N}(2, 1)$.

- For *non-additive noise neural network (NN) models* , we also follow the setup in (Brouillard et al., 2020; Lippe et al., 2021). We generate the data as $X_{n,:} = F_{n,:}(X, Z_{n,:})$, such that F is fully connected neural network, the weights are randomly initialized from $\mathcal{N}(0, 1)$. The neural network has one hidden layer with 20 hidden units, the activation function is a tanh function. The noise variables are sampled from $\mathcal{N}(0, \sigma^2)$, where $\sigma^2 \sim \mathcal{U}[1, 2]$. For nodes with interventions, values are sampled from the uniform distribution $\mathcal{N}(2, 1)$.

- For *MLP data*, the neural network has two fully connected layers of hidden dimensionality 32. Following past work (Ke et al., 2020a; Scherrer et al., 2021; Lippe et al., 2021), we used a randomly initialized network. For nodes with interventions, values are randomly and independently sampled from $U\{1, \ldots, K\}$ where K indicates the number of categories of the discrete variable.

- For Dirichlet data, the generator filled in the rows of a conditional probability table by sampling a categorical distribution from a Dirichlet prior with symmetric parameters α. Values of α smaller than 1 encourage lower entropy distributions; values of α greater than 1 provide less information about the causal relationships among variables. Similar to MLP data, for nodes with interventions, values are randomly and independently sampled from $U\{1, \ldots, K\}$ where K indicates the number of categories of the discrete variable.

A.3 Hyperparameters

Table 3: Hyperparameters used in all of our experiments.

Hyperparameter	**Value**
Hidden state dimension	128
Encoder transformer layers	10
Num. attention heads	8
Optimizer	Adam
Learning rate	$1e^{-4}$
Number of random seeds	3
S (number of samples)	1500
Training iterations	$50,000$
Num. training datasets I	$15,000$ $_{(N \leq 20)}$ $40,000$ $_{(N > 20)}$

For all of our experiments (unless otherwise stated) our model was trained on $I = 15,000$ (for graphs $N \leq 20$) and on $I = 40,000$ (for graphs $N > 20$) pairs $\{(\mathcal{D}^i, A^i)\}_{i=1}^{I}$, where each dataset $\mathcal{D}^i$ contained $S = 1500$ observational and interventional samples. For experiments on discrete data, a data-sample element x^s could take values in $\{1, 2, 3\}$. Details of the data generating process can be found in Section 4. For evaluation in Sections 6.1 and 6.2, our model was tested on $I' = 128$ (different for the training) pairs $\{(\mathcal{D}^{i'}, A^{i'})\}_{i'=1}^{I'}$, where each dataset $\mathcal{D}^{i'}$ contained $S = 1500$ observational and *interventional* samples. For the Asia, Sachs and Child benchmarks, our model was still tested on $I' = 128$ (different for the training) pairs $\{(\mathcal{D}^{i'}, A^{i'})\}_{i'=1}^{I'}$, however, $A^{i'} = A^{j'}$ since there is only a single adjacency matrix in each one of the benchmarks. We present test results averaging performance over the 128 datasets and 3 random seeds and up to size $N = 80$ graphs. The model was trained for $500,000$ iterations using the Adam optimizer (Kingma & Ba, 2014) with a learning rate of $1\text{e}{-4}$. Also, refer to Table 3 for the list of hyperparameters presented in a table.

We parameterized our architecture such that inputs to the encoder were embedded into 128-dimensional vectors. The encoder transformer has 10 layers and 8 attention-heads per layer. The final attention step for summarization has 8 attention heads. The decoder was a smaller transformer with only 2 layers and 8 attention heads per layer. Discrete inputs were encoded using an embedding layer before passing into our model.

A.4 COMPARISONS TO BASELINES

In Section 6.1, we compare CSIvA to four strong baselines in the literature, ranging from classic causal discovery baselines to neural-network based causal discovery baselines. These baselines are DAG-GNN (Yu et al., 2019), non-linear ICP (Heinze-Deml et al., 2018b), DCDI (Brouillard et al., 2020) and ENCO Lippe et al. (2021).

Non-linear ICP, DCDI and ENCO can handle both observational and *interventional* data, while DAG-GNN can only use observational data. Non-linear ICP could not scale to graphs larger than 20, therefore we compare to DCDI Brouillard et al. (2020) and ENCO Lippe et al. (2021) on larger graphs. All baselines are unsupervised methods, i.e. they are not tuned to a particular training dataset but instead rely on a general-purpose algorithm. We also compared to an all-absent model corresponding to a zero adjacency matrix, which acts as a sanity check baseline. We also considered other methods (Chickering, 2002; Hauser & Bühlmann, 2012; Zhang et al., 2012; Gamella & Heinze-Deml, 2020), but only presented a comparison with DCDI, ENCO, non-linear ICP and DAG-GNN as these have shown to be strong performing models in other works (Ke et al., 2020a; Lippe et al., 2021; Scherrer et al., 2021).

For Section 6.3, we also compared to additional baselines from Chickering (2002); Hauser & Bühlmann (2012); Zheng et al. (2018); Gamella & Heinze-Deml (2020); Li et al. (2020). Note that methods from Chickering (2002); Zheng et al. (2018); Yu et al. (2019); Li et al. (2020) take observational data only. DAG-GNN outputs several candidate graphs based on different scores, such as evidence lower bound or negative log likelihood, DCDI can also be run in two different settings (DCDI-G and DCDI-DSF), we chose the best result to compare to our model. Note that non-linear ICP does not work on discrete data, i.e. on the MLP and Dirichlet data, therefore a small amount of Gaussian noise $\mathcal{N}(0, 0.1)$ was added to this data in order for the method to run.

A.5 DETAILED RESULTS FOR SECTION 6.1

We present detailed results for experiments in Section 6.1 are described in the tables below.

A.5.1 RESULTS ON LINEAR DATA

Results for comparions between our model CSIvA and baselines non-linear ICP (Heinze-Deml et al., 2018b), DAG-GNN (Yu et al., 2019), DCDI (Brouillard et al., 2020) and ENCO (Lippe et al., 2021) are shown in Table 4 for smaller graphs with $N \leq 20$ and Table 5 for larger graphs with $20 < N \leq 80$.

For smaller graphs with $N \leq 20$, all models that takes interventional data perform significantly better compared to DAG-GNN (Yu et al., 2019), which only takes observational data. CSIvA achieves Hamming distance $\mathcal{H} < 7$ on evaluated graphs up to size 20. Similar to previous findings (Yu et al., 2019; Ke et al., 2020a), larger and denser graphs are more challenging to learn. Non-linear ICP achieves fairly good performance on smaller graphs ($N \leq 10$), however, the performance drops quickly as size of graphs increases ($N > 10$). Also, note that Non-linear ICP can not scale to graphs larger than $N > 20$. It also required a modification[2] to the dataset wherein multiple samples were collected from the same modified graph after a point intervention (20 samples per intervention), while other methods only sampled once per intervention.

For larger graphs of $20 < N \leq 280$, we compare to strongest baselines: DCDI and ENCO. Results are found in Table 5. CSIvA significantly outperforms both DCDI and ENCO. The difference because more apparent as the size of the graphs grow ($N \geq 50$).

A.5.2 RESULTS ON ANM DATA

For additive noise non-linear model (ANM) data, we compare to the strongest baseline models: DCDI and ENCO on $N \leq 80$ graphs. Results are found in Table 6. CSIvA achives hamming distance $\mathcal{H} < 11$ on all graphs of size up to 80. Therefore, CSIvA significantly outperforms strong baseline models DCDI and ENCO on all graphs. This difference becomes more apparent on larger graphs of $N \geq 50$.

[2]Without this modification, the method achieved near chance performance.

	ER = 1				ER = 2			
	Var = 5	**Var = 10**	**Var = 15**	**Var = 20**	**Var = 5**	**Var = 10**	**Var = 15**	**Var = 20**
Abs.	2.50	5.00	7.50	10.00	5.00	10.00	15.00	20.00
DAG-GNN	2.71	4.76	7.71	11.32	5.20	8.81	17.81	22.21
Non-linear ICP	0.47	1.10	6.3	8.6	0.90	2.41	13.52	17.71
DCDI	0.23	0.78	4.51	6.21	0.92	2.01	8.12	12.59
ENCO	0.19	0.45	3.12	4.23	0.85	1.81	6.14	8.45
Our Model	**0.12** ± 0.03	**0.35** ± 0.05	**2.01** ± 0.07	**2.21** ± 0.07	**0.81** ± 0.05	**1.73** ± 0.04	**5.32** ± 0.19	**5.86** ± 0.21

Table 4: **Results on Continuous linear data**. Hamming distance $\mathcal{H}$ for learned and ground-truth edges on synthetic graphs, compared to other methods, averaged over 128 sampled graphs. The number of variables varies from 5 to 20, expected degree = 1 or 2, and the value of variables are drawn from $\mathcal{N}(0, 0.1)$. Note that for (Heinze-Deml et al., 2018b), the method required nodes to be causally ordered, and 20 repeated samples taken per intervention, as interventions were continuously valued. "Abs" baselines are All-Absent baselines, which is an baseline model that outputs all zero edges for the adjacency matrix. DCDI and ENCO are the strongest performing baselines. CSIvA outperforms all baselines (including DCDI and ENCO).

Dataset	**All-absent**	**DCDI**	**ENCO**	**CSIvA**
$N = 30, ER = 1$	15.0	4.4	11.3	**1.8**
$N = 30, ER = 2$	30.0	9.2	29.1	**5.6**
$N = 50, ER = 1$	25.0	18.1	27.5	**3.5**
$N = 50, ER = 2$	50.0	23.7	73.2	**11.7**
$N = 80, ER = 1$	40.0	29.5	39.2	**9.8**
$N = 80, ER = 2$	80.0	49.3	97.2	**19.6**

Table 5: **Results on Linear data on larger graphs.** Hamming distance $\mathcal{H}$ for learned and ground-truth edges on synthetic graphs, compared to other methods. The number of variables varies from 30 to 80, expected degree = 1 or 2. We compare to DCDI Brouillard et al. (2020) and ENCO Lippe et al. (2021) as they are the best performing baselines and they are able to handle larger graphs.

A.5.3 Results on NN data

Results for comparisons between CSIvA and strongest baselines DCDI and ENCO on non-additive noise non-linear (NN) data are found in Table 7. CSIvA achieves hamming distance $\mathcal{H} < 11$ on all graphs. Hence, CSIvA significantly outperforms DCDI and ENCO on all graphs. The differences grow larger as the size of the graph grows.

A.5.4 Results on MLP data

Results for comparisons between our model CSIvA and baselines non-linear ICP (Heinze-Deml et al., 2018b) and DAG-GNN (Yu et al., 2019) on MLP data are shown in Table 9. MLP data is non-linear and hence more challenging compared to the continuous linear data. Our model CSIvA significantly outperforms non-linear ICP and DAG-GNN. The difference becomes more apparent as the graph size grows larger and more dense.

A.5.5 Results on Dirichlet data.

We run two sets of experiments on Dirichlet data. The first set of experiments is aimed at understanding how different α values impact the performance of our model. In the second set of experiments, we compare the performance of our model to four strong baselines: DCDI Brouillard et al. (2020), ENCO Lippe et al. (2021), non-linear ICP Heinze-Deml et al. (2018b) and DAG-GNN Yu et al. (2019).

The results for the first set of experiments are shown in Table 11. Our model performs well on all graphs where $\alpha \leq 0.5$, and the performance starts to degrading as $\alpha = 1.0$. When $\alpha = 5.0$, our model is almost performing similarly to the All-absent model (outputting all zero edges). This is to be expected, as larger alpha values is less informative of the causal relationships between variables.

Dataset	All-absent	DCDI	ENCO	CSIvA
$N = 30, ER = 1$	15.0	3.1	14.7	**0.7**
$N = 30, ER = 2$	30.0	5.8	31.2	**2.1**
$N = 50, ER = 1$	25.0	7.8	25.6	**0.7**
$N = 50, ER = 2$	50.0	9.7	48.2	**3.2**
$N = 80, ER = 1$	40.0	16.9	39.7	**4.3**
$N = 80, ER = 2$	80.0	37.1	78.2	**10.6**

Table 6: **Results on continuous non-linear additive noise model (ANM) data with larger graphs.** Hamming distance $\mathcal{H}$ for learned and ground-truth edges on synthetic graphs, compared to other methods. The number of variables varies from 30 to 80, expected degree = 1 or 2. We compare to DCDI Brouillard et al. (2020) and ENCO Lippe et al. (2021) as they are the best performing baselines and they are able to handle larger graphs.

Dataset	All-absent	DCDI	ENCO	CSIvA
$N = 30, ER = 1$	15.0	3.9	14.7	**0.8**
$N = 30, ER = 2$	30.0	6.7	29.2	**2.1**
$N = 50, ER = 1$	25.0	9.4	23.5	**1.3**
$N = 50, ER = 2$	50.0	10.4	49.5	**3.3**
$N = 80, ER = 1$	40.0	19.5	39.2	**5.3**
$N = 80, ER = 2$	80.0	39.8	80.6	**10.5**

Table 7: **Results on continuous non-linear non-additive noise model (NN) data with larger graphs.** Hamming distance $\mathcal{H}$ for learned and ground-truth edges on synthetic graphs, compared to other methods. The number of variables varies from 30 to 80, expected degree = 1 or 2. We compare to DCDI Brouillard et al. (2020) and ENCO Lippe et al. (2021) as they are the best performing baselines and they are able to handle larger graphs.

For the second set of experiments, we compared CSIvA to non-linear ICP and DAG-GNN on graphs of size up to 20. To limit the number of experiments to run, we set $\alpha = 1.0$, as this gives the least amount of prior information to CSIvA. As shown in Figure 6, our model significantly outperforms non-linear ICP and DAG-GNN. Our model achieves $\mathcal{H} < 5$ on size 10 graphs, almost half of the error rate compared to non-linear ICP and DAG-GNN, both achieving a significantly higher Hamming distance ($\mathcal{H} = 9.3$ and $\mathcal{H} = 9.5$ respectively) on larger and denser graphs. Refer to Table 10 for complete sets of results.

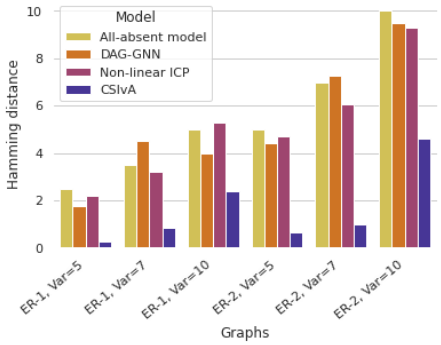

Figure 6: **Results on Dirichlet data on $N \leq 20$ graphs**. Hamming distance $\mathcal{H}$ between predicted and ground-truth adjacency matrices on Dirichlet data, averaged over 128 sampled graphs.

For larger graphs ($N > 20$), we compare CSIvA to DCDI Brouillard et al. (2020) and ENCO Lippe et al. (2021) as they could scale to larger graphs and are the strongest baselines. The results are illustrated in Figure 4 and the detailed results are found in Table 12. As the graphs get larger, the performance of baselines DCDI and ENCO drops significantly, for dense and largr graphs (ER-2, $N = 80$), the baseline models achieve almost near all-absent performance, while our model performs significantly better (achieving almost 30% performance gain in terms of structured hamming distance).

A.5.6 Soft Interventions

In addition to hard interventions, we also consider soft interventions. Hence, we further evaluate our model on imperfect interventions as discussed in Section 6.1. To limit the number of experiments to run, we focus on Dirichlet data with $\alpha = 0.1$ and $\alpha = 0.25$.

Dataset	All-absent	DCDI	ENCO	CSIvA
$N = 30, ER = 1$	15.0	11.1	12.5	**8.0**
$N = 30, ER = 2$	30.0	17.4	16.9	**15.6**
$N = 50, ER = 1$	25.0	27.3	28.3	**17.6**
$N = 50, ER = 2$	50.0	47.6	48.2	**33.6**
$N = 80, ER = 1$	40.0	52.8	35.8	**28.6**
$N = 80, ER = 2$	80.0	75.3	61.5	**52.3**

Table 8: **Results on discrete MLP data with larger graphs.** Hamming distance $\mathcal{H}$ for learned and ground-truth edges on synthetic graphs, compared to other methods. The number of variables varies from 30 to 80, expected degree = 1 or 2. We compare to DCDI Brouillard et al. (2020) and ENCO Lippe et al. (2021) as they are the best performing baselines and they are able to handle larger graphs.

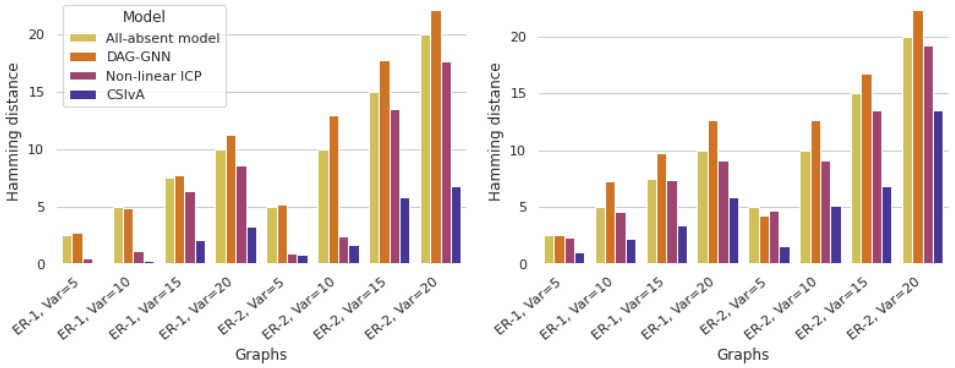

(a) **Results on Linear data on $N \leq 20$ graphs.** (b) **Results on MLP data on $N \leq 20$ graphs.**

Figure 5: Hamming distance $\mathcal{H}$ between predicted and ground-truth adjacency matrices on the Linear and MLP data for $N \leq 20$ graphs, compared to DAG-GNN (Yu et al., 2019) and non-linear ICP (Heinze-Deml et al., 2018b), averaged over 128 sampled graphs. CSIvA significantly outperforms all other baselines.

Soft interventions on Dirichlet data is generated as follows. For an intervention on variable X_i, we first sample the α_i for the Dirichlet distribution from a Uniform distribution $U\{0.1, 0.3, 0.5, 0.7, 0.9\}$, then using the sampled α_i, we sample the conditional probabilities from the Dirichlet distribution with the new α_i.

The results for CSIvA on soft interventions are shown in Table 13. CSIvA was able to achieve a hamming distance $\mathcal{H} < 5$ on all graphs of size $H \leq 20$. These results are strong indications that that our model still works well on the imperfect interventions.

A.5.7 Unknown Interventions

Until now, we have considered cases where the target of the intervention is known, we now consider the case when the target of the intervention is unknown, this is also referred to as unknown interventions. Again, to limit the number of experiments to run, we focus on Dirichlet data with $\alpha = 0.1$ and $\alpha = 0.25$. The model does not know the target of the intervention and all other training procedures remains exactly the same. The results are shown in Table 14. We compare how well CSIvAperforms on known and unknown interventions. We can see that the performance for the known and unknown interventions are almost the same for sparser graphs (ER-1). The differences increases slightly for denser graphs with higher values of α, for example $ER - 2$ graphs with $\alpha = 0.25$. This is to be expected, as denser graphs with higher α values are more challenging to learn. The biggest differences for the performances of known and unknown interventions is less than $\mathcal{H} < 1.0$ in hamming distance. These results shown clear indications that our model performs well even when the intervention target is unknown.

	ER = 1				ER = 2			
	Var = 5	**Var = 10**	**Var = 15**	**Var = 20**	**Var = 5**	**Var = 10**	**Var = 15**	**Var = 20**
Abs.	2.50	5.00	7.50	10.00	5.00	10.00	15.00	20.00
DAG-GNN	2.52	7.30	9.74	12.72	4.33	12.78	16.73	22.33
Non-linear ICP	2.43	4.62	7.42	9.05	4.76	9.12	13.52	19.25
CSIvA	**0.98** $\pm$ 0.16	**2.25** $\pm$ 0.17	**3.38** $\pm$ 0.12	**5.92** $\pm$ 0.19	**1.51** $\pm$ 0.47	**5.12** $\pm$ 0.26	**6.82** $\pm$ 0.23	**13.50** $\pm$ 0.35

Table 9: **Results on MLP data**. Hamming distance $\mathcal{H}$ for learned and ground-truth edges on synthetic graphs, compared to other methods, averaged over 128 sampled graphs ($\pm$ standard deviation). The number of variables varies from 5 to 20, expected degree = 1 or 2, and the dimensionality of the variables are fixed to 3. We compared to DAG-GNN (Yu et al., 2019), which is a strong baseline that uses observational data. We also compare to Non-linear ICP (Heinze-Deml et al., 2018b), which is a strong baseline that uses *interventional* data. Note that for (Heinze-Deml et al., 2018b), the method required nodes to be causally ordered, and Gaussian noise $\mathcal{N}(0, 0.1)$ to be added. "Abs" baselines are All-Absent baselines, which is an baseline model that outputs all zero edges for the adjacency matrix.

	ER = 1			ER = 2		
	Var = 5	**Var = 7**	**Var = 10**	**Var = 5**	**Var = 7**	**Var = 10**
All-absent baseline	2.5	3.5	5.0	5.0	7.0	10.0
(Yu et al., 2019)	1.75	4.5	4.0	4.5	7.25	9.50
(Heinze-Deml et al., 2018b)	2.2	3.2	5.3	4.7	6.1	9.3
CSIvA	**0.26** $\pm$ 0.05	**0.83** $\pm$ 0.06	**2.37** $\pm$ 0.07	**0.65** $\pm$ 0.05	**0.97** $\pm$ 0.06	**4.59** $\pm$ 0.08

Table 10: **Results on Dirichlet data.** Hamming distance $\mathcal{H}$ for learned and ground-truth edges on synthetic graphs, compared to other methods, averaged over 128 sampled graphs ($\pm$ standard deviation). The number of variables varies from 5 to 10, expected degree = 1 or 2, the dimensionality of the variables are fixed to 3, and the α is fixed to 1.0. We compare to the strongest causal-induction methods that uses observational data (Yu et al., 2019) and the strongest that uses *interventional* data (Heinze-Deml et al., 2018b).

A.6 Detailed results for Out-of-distribution experiments

This section contains detailed results for the out-of-distribution experiments experiments in Section 6.2. Results for the experiments on varying graph density in Section 6.2 are shown in Table 15 and Table 16. The results on varying α values in Section 6.2 are found in Table 17. Our model generalizes well to test OOD test distributions, where either the graphs can vary in terms of sparsity or the conditional probability can vary in terms of α values for the Dirichlet distributions.

A.7 Ablation studies and analyses

In order to better understand the performance of our model, we performed further analysis and ablations. This section contains full results for Section 6.4. In this section, we aim to answer the following questions:

- What does visualizations of the generated graphs look like?
- Are these generated graphs from our model acyclic?
- Does intervention data improve identifiability in our model?
- How does varying the number of samples impact the performance of our model?
- How does different components of our model (such as sample-level attention and auxiliary loss) impact the performance of our model?

A.7.1 Visualization of sampled graphs

	ER = 1				ER = 2			
	Var = 5	**Var = 10**	**Var = 15**	**Var = 20**	**Var = 5**	**Var = 10**	**Var = 15**	**Var = 20**
$\alpha = 0.1$	0.18± 0.03	0.72± 0.04	1.31± 0.04	2.45 ± 0.04	0.39± 0.04	1.27± 0.07	1.98± 0.12	4.09± 0.04
$\alpha = 0.25$	0.14± 0.03	0.77± 0.05	1.62± 0.05	3.51 ± 0.05	0.29± 0.04	1.27± 0.07	3.04± 0.20	6.41± 0.12
$\alpha = 0.5$	0.14± 0.04	0.94± 0.05	4.26± 0.07	7.35± 0.04	0.41 ± 0.03	2.11± 0.06	8.25± 0.07	15.54± 0.10
$\alpha = 1.0$	0.26± 0.05	2.37± 0.07	4.90± 0.05	10.10± 0.07	0.68± 0.03	4.32± 0.07	10.24± 0.07	21.81± 0.07
$\alpha = 5.0$	1.27± 0.12	4.9± 0.05	14.73± 0.11	19.49± 0.05	3.21± 0.05	9.99 ± 0.03	24.19± 0.05	37.03± 0.24
Abs.	2.5	5.0	7.5	10.0	5.0	10.0	15.0	20.0

Table 11: **Results on Dirichlet data.** Hamming distance $\mathcal{H}$ (lower is better) for learned and ground-truth edges on synthetic graphs, averaged over 128 sampled graphs. Our model accomplished a hamming distance of less than 2.5 for Dirichlet data with $\alpha <= 0.5$. "Abs" baselines are All-Absent baselines, which is an baseline model that outputs all zero edges for the adjacency matrix.

Dataset	**All-absent**	**DCDI** Brouillard et al. (2020)	**ENCO** Lippe et al. (2021)	**CSIvA**
$N = 30, ER = 1$	15.0	8.3	4.9	**2.9**
$N = 30, ER = 2$	30.0	12.3	8.1	**6.5**
$N = 40, ER = 1$	20.0	16.2	9.9	**5.3**
$N = 40, ER = 2$	40.0	21.6	14.3	**9.6**
$N = 50, ER = 1$	25.0	26.4	17.7	**8.9**
$N = 50, ER = 2$	50.0	47.6	28.6	**17.3**
$N = 60, ER = 1$	30.0	28.4	25.6	**12.6**
$N = 60, ER = 2$	60.0	57.6	38.2	**26.6**
$N = 70, ER = 1$	35.0	34.1	29.1	**18.4**
$N = 70, ER = 2$	70.0	71.2	53.4	**40.9**
$N = 80, ER = 1$	40.0	54.1	39.1	**23.1**
$N = 80, ER = 2$	80.0	78.6	72.6	**56.3**

Table 12: **Results on Dirichlet data with larger graphs.** Hamming distance $\mathcal{H}$ for learned and ground-truth edges on synthetic graphs, compared to other methods. The number of variables varies from 30 to 80, expected degree = 1 or 2, and the α is fixed to 0.1. We compare to the approaches from Brouillard et al. (2020) and Lippe et al. (2021) as they are the strongest baselines and they are able to handle larger graphs.

We visualized samples that our model generated on the test data. The samples are shown in Figure 9 and Figure 8. The samples are randomly chosen, each subplot is a sample from a distinct test data. The edges in the graph are shown in 3 colors, they each represent the following: (a) Green edges indicate that our model has generated the correct edge. (b) A red edge indicates a missing edge, that is our model did not generate the edge, which exist in the groundtruth graph. (c) A blue edge indicates a redundant edge, such that our model generated an edge that does not exist in the groundtruth graph. As shown in Figure 9 and 8, our model is able to generate the correct graph almost all of the times.

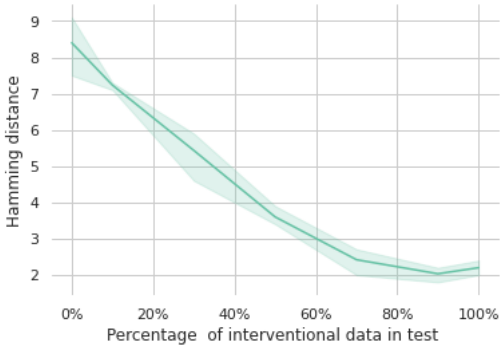

Figure 7: **Results on varying amount of interventions in data.** Hamming distance $\mathcal{H}$ for learned and ground-truth edges on synthetic Dirichlet graphs ($Var = 15$ and $\alpha = 0.25$). Pure observational data (0% interventions) performs the worst, which is to be expect, since intervention data is need for causal identifiability. The performance of our model improves as it observes more interventions, this suggest that our model is able to extract useful information from interventions in order to predict the causal structure.

A.7.2 Acyclicity of generated graphs

As discussed in Section 6.4, we analyzed the generated graphs for acyclicity on Dirichlet data with $\alpha = 0.1$ and $\alpha = 0.25$ for graphs of size up to $N \leq 20$. We evaluated the model on 128 test datasets per setting, and found that none of

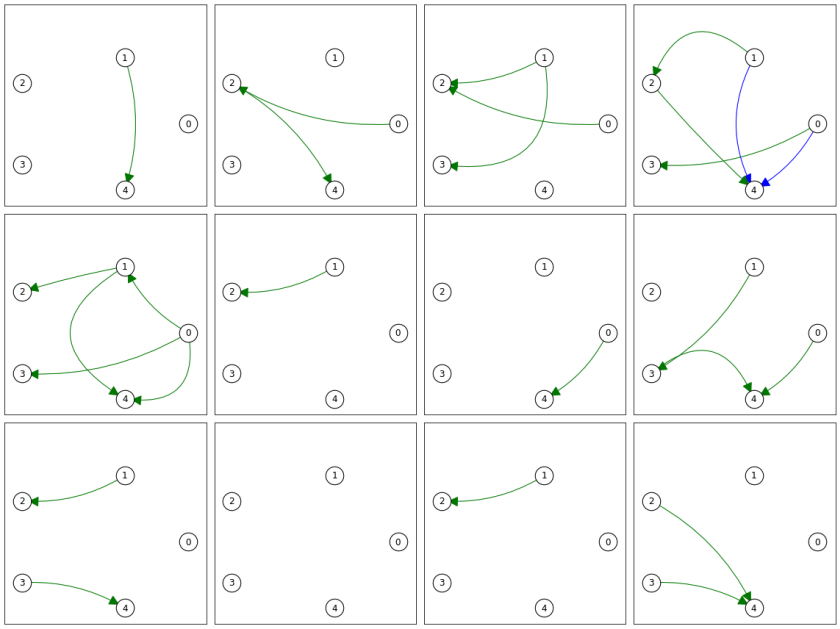

Figure 8: This figures visualizes samples that our model generated on test data. The model was trained and tested on MLP data of size 5 with **ER-**1 graphs. The samples are randomly chosen. The green edges indicate that our model has generated the correct edges; red edges indicate edges that our model had missed; and blue edges are the ones that our model generated, which were not in the groundtruth graph. As shown above, our model is able to generate the correct graph almost all of the times, while only occasionally generating 1 or 2 incorrect edges in a graph.

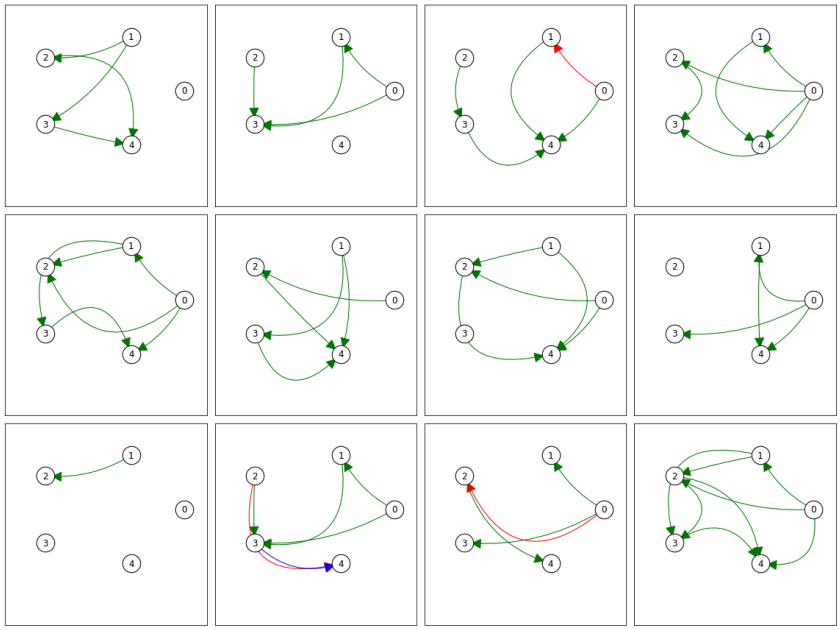

Figure 9: This figures visualizes samples that our model generated on test data. The model was trained and tested on MLP data of size 5 with **ER-**2 graphs. The samples are randomly chosen. The green edges indicate that our model has generated the correct edges; red edges indicate edges that our model had missed; and blue edges are the ones that our model generated, which were not in the groundtruth graph. As shown above, our model is able to generate the correct graph almost all of the times, while only occasionally generating 1 or 2 incorrect edges in a graph.

	ER = 1			ER = 2		
	Var = 10	**Var = 15**	**Var = 20**	**Var = 10**	**Var = 15**	**Var = 20**
All-absent baseline	5.0	7.5	10.0	10.0	15.0	20.0
$\alpha = 0.1$	0.5	1.2	2.4	0.9	2.3	3.4
$\alpha = 0.25$	0.5	1.7	3.3	1.7	3.5	4.6

Table 13: **Results on imperfect interventions.** Hamming distance $\mathcal{H}$ for learned and ground-truth edges on synthetic graphs, compared to other methods, averaged over 128 sampled graphs ($\pm$ standard deviation). The number of variables varies from 10 to 20, expected degree = 1 or 2, the dimensionality of the variables are fixed to 3, and the α is fixed to 0.1 or 0.25.

	ER = 1				ER = 2			
	Var = 15		**Var = 20**		**Var = 15**		**Var = 20**	
	$\alpha = 0.1$	$\alpha = 0.25$	$\alpha = 0.1$	$\alpha = 0.25$	$\alpha = 0.1$	$\alpha = 0.25$	$\alpha = 0.1$	$\alpha = 0.25$
Known	1.3	1.7	2.5	3.4	2.3	3.0	4.1	6.3
Unknown	1.4	1.9	2.5	3.3	2.3	3.5	4.1	6.6

Table 14: **Results on unknown interventions compared to known interventions.** Hamming distance $\mathcal{H}$ from learned and ground-truth edges on synthetic graphs, for known vs unknown interventions, averaged over 128 sampled graphs ($\pm$ standard deviation). The number of variables varies from 15 to 20, expected degree = 1 or 2, α = 0.1 or 0.25, and the dimensionality of the variables are fixed to 3.

the generated graphs contains cycles, all graphs
are acyclic. This is a clear indication showing that although we do not have an acyclicity regularizer, our model was still able to learn to generated DAGs.

A.7.3 Identifiability upon seeing intervention data.

Our previous experiments were all performed using a fixed amount of interventions (80%) in the training and test sets. To investigate how changing the proportion of interventional data impacts the performance of our model, we train the model with varying amounts of interventions in the training set and evaluate it using different amount of interventions during test time.

To be specific, during training, the model is trained on data with varying amount of interventions, which is randomly sampled from the uniform distribution $U[0, 0.1, 0.3, 0.5, 0.7, 0.9, 1.0]$. During test time, we evaluate the model on different amount of interventions, and we report the performance in hamming distance. We trained the model on Dirichlet data with 15 nodes and $\alpha = 0.25$. The model is trained and tested on 1000 samples per dateset. The results are found in Figure 7.

As shown in Figure 7, our model's performance is worst if it only receives observational data (0% interventions), and the performance of our model improves as the amount of interventional data

Train		ER-1	ER-2	ER-3
	ER-1	1.2	0.9	1.3
Test	ER-2	3.3	1.8	2.1
	ER-3	5.0	2.8	2.8

Table 15: **Results on varying graph density for MLP data:** Hamming distance $\mathcal{H}$ between predicted and ground-truth adjacency matrices.

Train		ER-1	ER-2	ER-3
	ER-1	0.19	0.21	0.28
Test		0.86	0.29	0.25
	ER-3	1.61	0.60	0.23

Table 16: **Results on graph sparsity for Dirichlet data ($\alpha = 1$):** Hamming distance $\mathcal{H}$ between predicted and ground-truth adjacency matrices.

Train		$\alpha = 0.1$	$\alpha = 0.25$	$\alpha = 0.5$
	$\alpha = 0.1$	0.31	0.33	0.52
Test	$\alpha = 0.25$	0.72	0.40	0.41
	$\alpha = 0.5$	1.8	0.71	0.35

Table 17: **Results on varying α values for Dirichlet data:** Hamming distance $\mathcal{H}$ between predicted and ground-truth adjacency matrices.

increases. This is a clear indication that our model is able to extract information from interventional data for predicting the graph structure.

A.7.4 Varying number of samples

We evaluated CSIvA on different amount of samples $(100, 200, 500, 1000, 1500)$ per CBNs. To limit the number of experiments to run, we focus on Dirichlet data sampled from $N = 10$ graphs. During the ith iteration in training, the model takes in as input a dataset with l_i samples, where l_i is sampled from $U[100, 200, 500, 1000, 1500]$. During test time, we run separate evaluations on the model for test datasets with different number of samples and the results are reported in Figure 10. We can see that the model performance improves as it observes up to 1000 samples for ER-1 graphs, whereas having 1500 samples gives slightly better results compared to 1000 samples for ER-2 graphs.

A.7.5 Ablation studies

We investigate the role that different components play in our model, for example, what are the effects of having auxillary loss and sample-level attention for our model. The details for each experiment is described below.

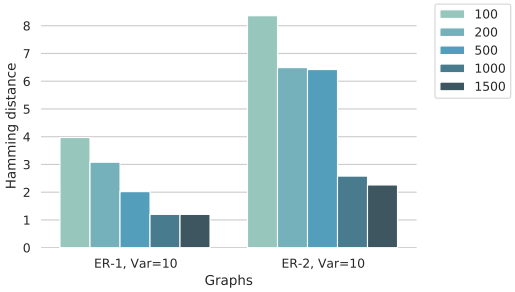

Figure 10: **Results on varying number of samples**. Hamming distance $\mathcal{H}$ between predicted and ground-truth adjacency matrices for synthetic data. Results for CSIvA trained on Dirichlet data with $N = 10$ and $\alpha = 0.5$ with different numbers of samples per CBNs. The model performance increases as the sample size increases.

Sample-level attention We first evaluated the performance of our with and without sample-level attention. In the case without sample-level attention, our model will only use node-level attention for all 10 layers in the encoder transformer. The results are reported in Table 18. The models with sample-attention is a vanilla CSIvA model; and the model without sample-attention is CSIvA without sample-level attention. As one could see that the performance of the model drops significantly if sample-attention is not used. Hereby making sample-level attention a crucial component in our model.

Auxiliary loss We also conducted ablation studies to understand the effect of the auxiliary loss in the objective function, results are reported in Table 19. The model with auxiliary loss is the vanilla CSIvA model, where as the one without is CSIvA trained without the auxiliary loss objective. Experiments are conducted on Dirichlet data with $\alpha = 0.1$, the model does gain a small amount of performance (H< 1.0) by having the auxiliary loss, the difference becomes more apparent as the size of the graph grows, indicating that auxiliary loss plays an important role as a part of the objective function.

	ER = 1				**ER = 2**			
	Var = 15		**Var = 20**		**Var = 15**		**Var = 20**	
	$\alpha = 0.1$	$\alpha = 0.25$	$\alpha = 0.1$	$\alpha = 0.25$	$\alpha = 0.1$	$\alpha = 0.25$	$\alpha = 0.1$	$\alpha = 0.25$
Sample attention	1.3	1.7	2.5	3.4	2.3	3.0	4.1	6.3
No sample attention	15.3	15.5	21.8	22.4	29.3	29.7	39.4	40.0

Table 18: Results for CSIvA with and without **sample-level attention**. Hamming distance $\mathcal{H}$ from learned and ground-truth edges on synthetic graphs, for known vs unknown interventions, averaged over 128 sampled graphs ($\pm$ standard deviation). The number of variables varies from 15 to 20, expected degree = 1 or 2, α = 0.1 or 0.25, and the dimensionality of the variables are fixed to 3.

	ER = 1		**ER = 2**	
	Var = 15	**Var = 20**	**Var = 15**	**Var = 20**
Aux loss	1.2	2.4	2.3	3.4
No aux loss	1.8	3.1	2.8	4.5

Table 19: Results for CSIvA trained with and without **auxiliary loss**. Hamming distance $\mathcal{H}$ from learned and ground-truth edges on synthetic graphs, for known vs unknown interventions, averaged over 128 sampled graphs ($\pm$ standard deviation). The number of variables varies from 15 to 20, expected degree = 1 or 2, α = 0.1, and the dimensionality of the variables are fixed to 3.